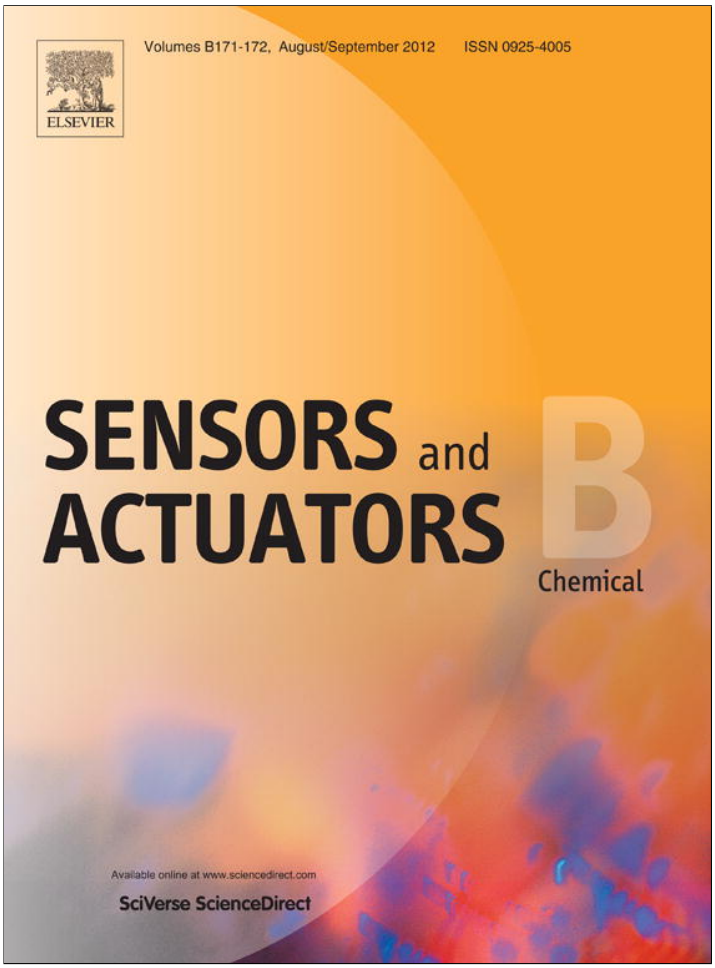

Sensors and Actuators B 171–172 (2012) 238–243

Contents lists available at SciVerse ScienceDirect

Sensors and Actuators B: Chemical

journal homepage: www.elsevier.com/locate/snb

Highly sensitive electrolyte-insulator-semiconductor pH sensors enabled by silicon nanowires with Al_2O_3/SiO_2 sensing membrane

Jin Yong Oh [a], Hyun-June Jang [b], Won-Ju Cho [b], M. Saif Islam [a,*]

[a] Department of Electrical and Computer Engineering, University of California Davis, One Shields Avenue, Davis, CA 95616, United States
[b] Department of Electronic Materials Engineering, 447-1, Wolgye-dong, Nowon-gu, Seoul 139-701, South Korea

ARTICLE INFO

Article history:
Received 17 January 2012
Received in revised form 12 March 2012
Accepted 18 March 2012
Available online 28 March 2012

Keywords:
EIS
ISFET
pH sensor
Chemical sensor
Silicon
Nanowires

ABSTRACT

Low sensitivity and poor reliability currently limit the applications of solid-state bio-chemical sensors. We demonstrate an electrolyte-insulator-semiconductor (EIS) sensor with a large capacitance, near-Nernst-limit pH sensitivity, and good reliability by integrating an ensemble of Si nanowires (NWs) for the first time. The NWs were fabricated by using the electroless wet etching technique. An Al_2O_3/SiO_2 bilayer coating was employed as a sensing membrane. The EIS sensors with 3.8 μm long NWs exhibited about 8 times larger capacitance than that of a planar type EIS sensors that were fabricated using the same fabrication scheme without integrating NWs. The measured pH sensitivity at room temperature was 60.2 mV/pH, which is higher than the theoretical Nernstian of 59 mV/pH. Our results and analysis clearly indicate that ultra-sensitive pH sensing can be realized with optimized NW integrated EIS sensors.

Ion-sensitive field effect transistors (ISFETs) have been attracting considerable interests as bio-chemical and pH sensors since they were first demonstrated by Bergveld in 1970s [1–3]. Electrical potential generated by ions at the interface of gate dielectric and electrolyte modulates the channel current of the sensors, which is similar to the operating mechanism of the conventional metal-oxide-semiconductor field effect transistors (MOSFETs). Electrolyte-insulator-semiconductor (EIS) sensor is the most basic of all ISFET devices. It is a capacitive field effect device, which monitors the chemical changes such as pH fluctuation by capacitance measurement [4]. The simple and inexpensive fabrication scheme of the EIS sensors makes them attractive candidates as bio-chemical sensors as well as preliminary devices of ISFET for evaluating the characteristics of membranes such as capacitance, pH sensitivity, hysteresis, and drift.

In spite of several interesting demonstrations showing the potential of EIS and ISFET sensors, some performance-limiting challenges need to be addressed for large scale implementation of the devices. These include achieving a large gate capacitance and increasing the pH sensitivity close to the theoretical limit, the Nernstian of 59 mV/pH. Poorer sensitivity impedes the detection of minute variation of the environment. Small gate capacitance exhibited by the typical devices poses a device miniaturization challenge. For analog devices such as ISFET sensors, the ability to sense a small magnitude of current variation is critical, because signal-to-noise ratio determines the accuracy of the devices.

To address the aforementioned weaknesses, several kinds of high-k dielectrics and other engineered dielectrics have been studied as sensing membrane [5–13]. Properties of the dielectric membrane are the primary factor to determine sensing capability of the sensors. The high-k dielectric membranes are helpful in not only increasing capacitance of the device and pH sensitivity, but also reinforcing their immunity to non-ideal effects such as hysteresis and drift [6,7,10]. Post deposition annealing process of high-k dielectrics was reported to be useful to increase pH sensitivity due to the increased surface roughness of the sensing membrane [10,11]. Another approach to increase capacitance and sensitivity was to expand the surface area of the sensing window in the devices using 3-D structures. For example, porous silicon sensors showed a considerably increased maximum capacitance as well as improved pH sensitivity [14–16]. In the recent past, researcher have seen the elucidation of complex heterogeneous fabrication methods that have emerged to the point that a remarkable degree of technical precision is achieved in the ISFET designs contributing to ultra-high capacitance as well as unprecedented sensitivity. For example, the application of dual-gate FETs and other approaches helped in increasing the sensitivity to close to or above the Nernst-limit [17–19].

* Corresponding author. Tel.: +1 530 754 6732.
E-mail address: sislam@ucdavis.edu (M.S. Islam).

0925-4005/$ – see front matter © 2012 Elsevier B.V. All rights reserved.
doi:10.1016/j.snb.2012.03.052

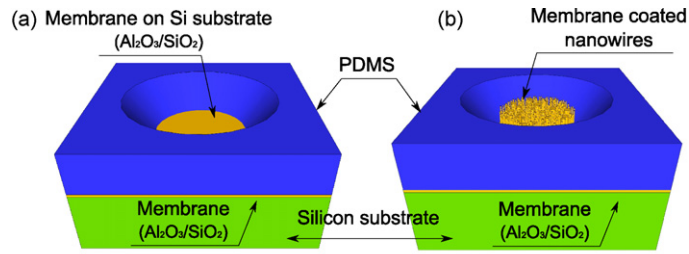

Fig. 1. Schematic diagrams of (a) the planar EIS sensor and (b) NW integrated EIS sensor, respectively.

In this work, integration of NWs and Al_2O_3/SiO_2 stacked sensing membrane into EIS sensors was demonstrated to address both of the aforementioned major weaknesses of the EIS sensors. The significantly increased surface area of NWs and the high permittivity of Al_2O_3 performed as expected and enhanced both the capacitance and pH sensitivity of the EIS sensor. Sensors with integrated longer NWs exhibit increased capacitance and pH sensitivity. We also present non-ideal properties in order to evaluate performance of the EIS sensors with NWs.

Silicon NWs were prepared on p-type (1 0 0) Si wafers (resistivity of 1–10 Ω cm) by the electroless wet chemical etching method. The surface of Si wafers was pre-cleaned by the conventional standard cleaning method. A wet etching solution was prepared with $AgNO_3$ of 0.25 M/L and HF of 4.6 M/L as described in a reference [20]. Four kinds of EIS sensors with NWs of 0.4 μm, 0.9 μm, 1.8 μm, and 3.8 μm were prepared by controlling the wet etch time at room temperature (RT). Then, the wafers were post-cleaned in a fuming nitric acid for an hour to remove silver dendrites and residual ions. Subsequently, additional cleaning processes were applied to all the wafers using piranha (1:1 solution of 97% H_2SO_4 and 30% H_2O_2), 6:1 buffered oxide etchant, and deionized water rinsing, each for 10 min in sequence. For the comparison, a conventional planar type EIS sensor without NWs was fabricated simultaneously with the NW EIS sensors.

As a sensing membrane, 17.8 nm thick thermal SiO_2 and 24.6 nm thick Al_2O_3 deposited by atomic layer deposition (ALD) were sequentially grown on silicon NWs. As a metal backside contact, a 300 nm thick Al film was deposited by e-beam evaporation on the backside of the Si substrates after oxide removal. All the devices were followed by a post annealing process at 450 °C for 30 min in the forming gas (mixture of 2% H_2 in N_2). The morphology and detailed structures of Al_2O_3/SiO_2 membrane coated NWs were characterized by FEI 430 scanning electron microscope (SEM) and Philips CM120 transmission electron microscope (TEM).

EIS sensors were fabricated with polydimethylsiloxane (PDMS) reservoirs with a 7 mm diameter hole upon 1 cm × 1 cm specimens cut from the NW grown substrates. A commercial Ag/AgCl reference electrode and HP4284A LCR meter were employed to measure the *C–V* characteristics of EIS sensors. Detailed measurement principle and configuration are introduced in elsewhere [4]. For the *C–V* measurement, a low frequency of 100 Hz was applied in order to maintain the electrochemical equilibrium. All of the sensors were immersed in reversed osmosis water for 12 h prior to the *C–V* measurement for steady pH responses. The pH buffer solutions were kept at 21 °C, and measurements were executed in a dark shield box at the same temperature.

Fig. 1 presents schematics of the conventional planar type EIS sensor and the sensor incorporated with NWs, respectively. The basic structures of the two sensors are identical except that the NW EIS sensors have additional NWs in the pH sensing area to increase the surface area. In Fig. 2, a TEM image of a NW harvested from the EIS sensor with 0.9 μm NWs clearly shows the final structure

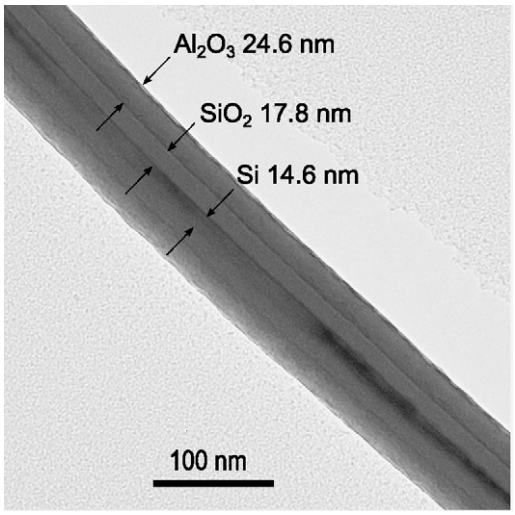

Fig. 2. TEM image of an Al_2O_3/SiO_2 membrane coated NW. Thickness of remaining silicon core, SiO_2 and Al_2O_3 was displayed from inside to outside of the NW.

of the NW with a remaining Si core of 14.6 nm and a homogeneous membrane shell composed of thermal SiO_2 of 17.8 nm and ALD Al_2O_3 of 24.6 nm. Even for NWs longer than 3.8 μm, the Al_2O_3 membrane was homogeneously coated all along the NWs. Thermal oxidation consumed 12.3 nm of Si from the surface of the NWs to grow 17.8 nm thick SiO_2. Thus, the thinner NWs with thickness less than about 12.3 nm should be fully oxidized. Cross-sectional SEM images in Fig. 3 show the uniform distribution of Al_2O_3/SiO_2 membrane coated NWs of four different lengths on silicon wafers. The morphology of membrane coated NWs are almost identical to that of NWs before membrane coating, because thermal oxidation and ALD for Al_2O_3 deposition form very conformal membrane layers. Statistical lengths and diameters of NWs of all the EIS sensors are shown in Table 1.

To evaluate the effect of NWs on the characteristics of EIS sensor, first of all, the capacitance of EIS sensors with different lengths of NWs were compared with that of the control device, planar type EIS sensor. The capacitance was measured by sweeping voltages at the substrate electrode using a pH 7 buffer solution. As shown in Fig. 5

Table 1
Data of statistical NW measurement, estimated area fraction, and increased surface area of NWs of 0.4 μm, 0.9 μm, 1.8 μm and 3.8 μm.

NW length (μm)	Average radius (nm), standard deviation (nm)	Area fraction (%)	Increased surface area/inspection area
0.4	122.1, 49.3	31.8	2.1
0.9	109.2, 52.9	35.7	5.9
1.8	121.8, 34.8	31.5	9.3
3.8	116.4, 27.5	24.9	16.3

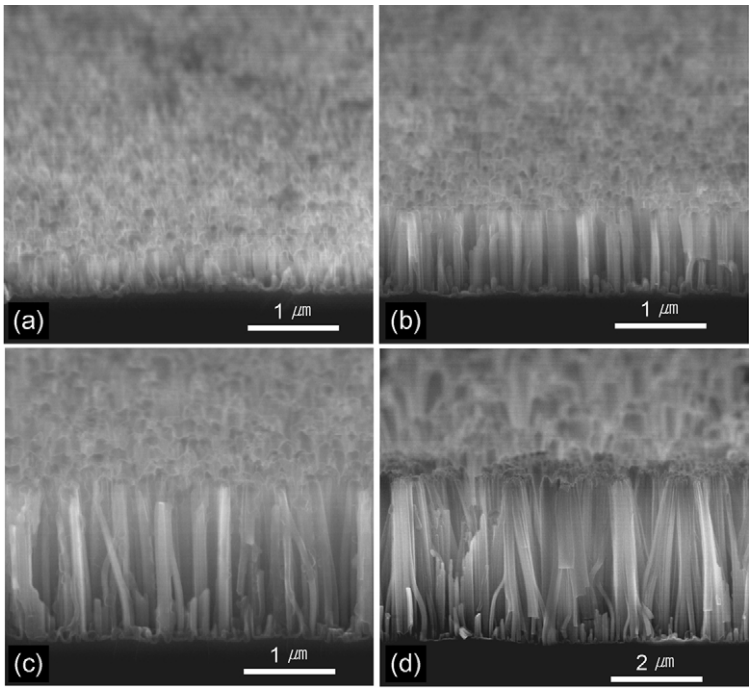

Fig. 3. Cross-sectional view SEM images of Al_2O_3/SiO_2 membrane coated NWs of (a) 0.4 μm, (b) 0.9 μm, (c) 1.8 μm, and (d) 3.8 μm NWs.

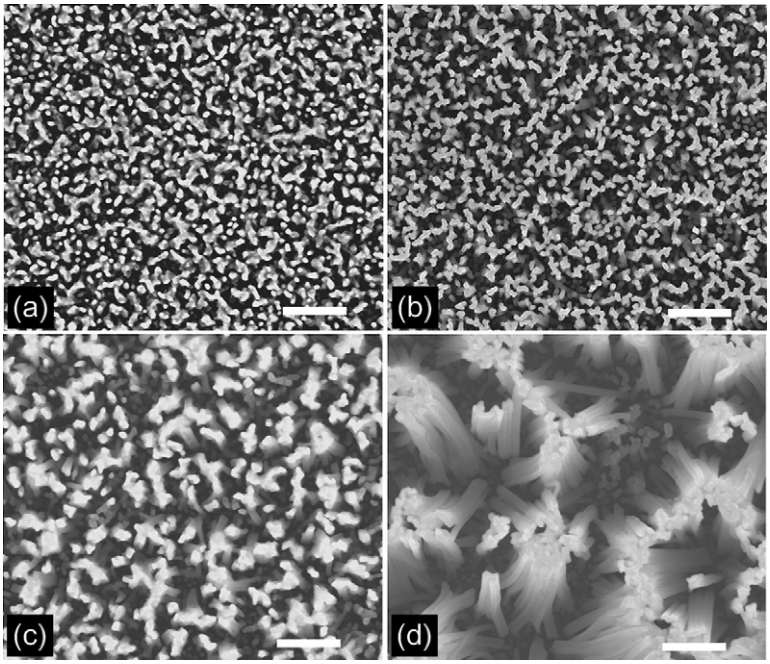

Fig. 4. Plan view SEM images of Al_2O_3/SiO_2 membrane coated NWs of (a) 0.4 μm, (b) 0.9 μm, (c) 1.8 μm, and (d) 3.8 μm. The size of scale bars is 1 μm.

and summarized in Table 2, all the NW integrated EIS sensors exhibited higher maximum capacitance at the accumulation regime than that of the planar type sensor. Maximum capacitance of the planar type sensor was 98 nF. On the other hand, the capacitances of the NW integrated sensors were 257 nF, 465 nF, 767 nF, and 870 nF with 0.4 μm NWs, 0.9 μm NWs, 1.8 μm NWs, and 3.8 μm NWs, respectively. Capacitance of the EIS sensor directly affects the magnitude of sensing current in ISFET as described by $I_{sensing} \propto C_{OX}W/L$, where C_{OX} is the capacitance of the gate dielectric material, and W and L are width and length of the gate. Consequently, integration of NWs into ISFET sensors would improve the signal-to-noise margin.

Table 2
Summary of measured characteristics of the EIS sensors.

Device type	Capacitance max (nF)	pH sensitivity (mV/pH)	Linearity of pH sensitivity (%)	Hysteresis (mV)
Planar	98	54.9	99.9	5.5
0.4 μm NW	257	55.4	99.7	8.3
0.9 μm NW	465	58.3	99.7	25.0
1.8 μm NW	767	59.5	99.8	5.3
3.8 μm NW	870	60.2	99.4	22.4

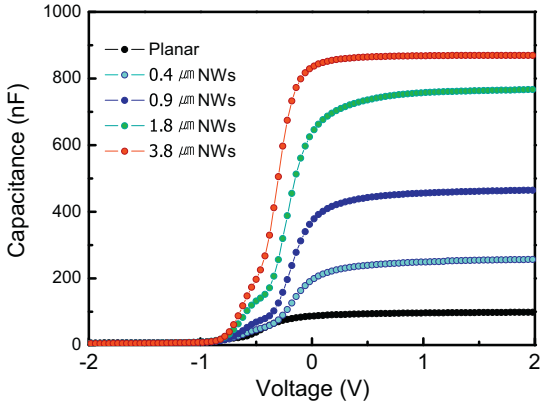

Fig. 5. *C–V* characteristics of the NW EIS sensors and the planar type EIS sensor.

The increase in capacitance is explainable by the increase in the surface area of NWs. The surface area proportionally varies with the density and length of NWs. That is, the increased surface area enabled by NWs is given by $n \times 2\pi R \times L$, where n is the number of NWs in a plan view SEM image, R is an average radius of NWs, and L is an average length of NWs. We can calculate the increased surface area with following relationships. The top surface area of NWs in the SEM image is given by $n \times \pi R^2$, which can be estimated by calculating an area fraction. The area fraction is the ratio of top surface area occupied by NWs to the entire area of the SEM image. Area fractions given in Table 1 are average values obtained from 4 different magnification top view SEM images (×10,000, ×25,000, ×50,000, ×100,000) using a software, "Image-J". From the relationship between the increased surface area by NWs and measured top area of NWs, given by

$$\frac{\text{Increased surface area}}{\text{Top surface area of NWs}} = \frac{\text{Increased surface area}}{\text{Area fraction} \times \text{SEM image area}} = \frac{n \times 2\pi R \times L}{n \times \pi R^2}$$

we can get the increased surface area as

$$\frac{\text{Increased surface area}}{\text{SEM image area}} = \text{Area fraction} \times \frac{L}{R}.$$

As shown in Table 1, the increased surface area of sensors by integrating NWs are almost proportional to the length of NWs. Longer NWs, however, become less mechanically stiff, so they tend to bend. In addition, van der Waals force between NWs helps them to stick together for clusters [21] as shown in Fig. 4. The EIS sensors with longer NWs, therefore, did not show a proportional increase in the maximum capacitance to the length or increased surface area of the NWs. Besides, the EIS sensors with NWs longer than 4 μm yielded poor *C–V* characteristics because of leakage current presumably contributed by long NWs that broke off due to mechanical stress and vibrations during the sample.

pH sensing capability of EIS sensors can be characterized by using *C–V* measurements. Fig. 6a shows normalized *C–V* curves of the EIS sensor with 0.9 μm NWs in different pH solutions. The flatband of *C–V* curves is found to shift in a parallel configuration due to the pH change in the solutions. The shift of the *C–V* curves can be explained by the surface potential variation of the sensor enabled by the surface ionization with H^+ or OH^- ions. The *C–V* curves were obtained by sweeping voltages at the backside contact and setting the reference electrode as a ground in several different pH solutions. All the other EIS sensors with varying NW lengths as well as the planar type devices also showed similar characteristics (not shown here). Fig. 6b shows the pH dependency of reference voltages for all of the EIS sensors. The reference voltage, which is defined as a voltage for the half maximum of the normalized capacitance, was extracted from the *C–V* curves. Although the pH dependency curves of the sensors with NWs show slightly degraded linearity than the planar EIS sensor, they exhibit excellent linearity of higher than 99.0%, which is satisfactory enough to calculate the pH sensitivity of the sensors.

The increased surface area enabled by NWs integrated into EIS sensors improves not only the maximum capacitance, but also the pH sensitivity of sensors as summarized in Table 2. The pH sensitivity of the planar type EIS sensor was measured to be 54.9 mV/pH. On the other hand, the devices with 0.4 μm NWs showed an increased sensitivity of 55.4 mV/pH. Considerably improved pH sensitivity, 59.5 mV/pH and 60.2 mV/pH, which are very close to the Nernstian at RT, were obtained from the devices with NWs of 1.8 μm and 3.8 μm, respectively. The effect of the increase in the surface area of EIS sensors on the improved pH sensitivity has been successfully explained by the surface binding model [10,22]. From the model, surface potential dependency of EIS on pH is described as,

$$\frac{d\psi}{d\text{pH}} = -2.303\frac{kT}{q}\frac{\beta}{\beta+1}$$

where $d\Psi/d$pH is potential variation by pH change; k is Boltzmann's constant; T is absolute temperature of the system; q is the electric charge; β is the parameter indicating the chemical sensitivity of the sensing membrane [23]. And, β is given as,

$$\beta = \frac{2q^2 N_s \sqrt{K_a K_b}}{kTC_{DL}}$$

where N_s is the total number of surface site per unit area; K_a is an equilibrium constant of acid point; K_b is an equilibrium constant of base point; C_{DL} is capacitance of the double layer in the electrolyte. The pH sensitivity becomes closer to the Nernstian when β is much larger than 1. Increasing N_s, therefore, is a straightforward way to improve pH sensitivity of EIS sensors with the assumption that equilibrium constants (K_a and K_b) and C_{DL} are negligibly changed by the increase in N_s. In practical devices, rough membrane surfaces generated by rapid thermal annealing and porous silicon surfaces fabricated by anodic etching showed improved pH sensing capability [15,22,24,25]. Similarly, in our NW integrated EIS sensors, significantly increased surface area enabled by the NWs evidently enhanced the pH sensitivity.

Despite an improvement in the pH sensitivity with increased NW length, the hysteresis properties of the EIS sensors became slightly worse with longer NWs as shown in Fig. 7a and Table 2. Hysteresis is one of the critical mechanisms that limit the accuracy of EIS or ISEFET sensors. In the past, Al_2O_3 membrane was employed in the EIS sensors because it is known to be a durable membrane with high immunity to hysteresis [26–28]. For the hysteresis measurement, the sensors were subjected to a pH loop of 7–10–7–4–7 over a period of 1 h, and the hysteresis voltages were calculated as a difference between the initial reference voltage and the final reference voltage at pH 7. As summarized in Table 2, the planar type EIS sensor shows the smallest value of 5.5 mV, while the EIS sensors with 0.4 μm, 0.9 μm, 1.8 μm, and 3.8 μm NWs show 8.3 mV, 25.0 mV, 5.3 mV, and 22.4 mV of hysteresis, respectively. Hysteresis is known to be related to chemical interaction between ions in an electrolyte and slow reacting surface-sites underneath the membrane surface and/or the surface defects of the membrane [7]. Larger surface area of longer NWs should contain more slow reacting-sites. Consequently, it is expected that hysteresis becomes poorer for the longer NW based devices.

The drift in the reference voltage of EIS or the threshold voltage of ISFET over a long time period poses a serious challenge in the widespread application of the solid state pH sensors. The drift

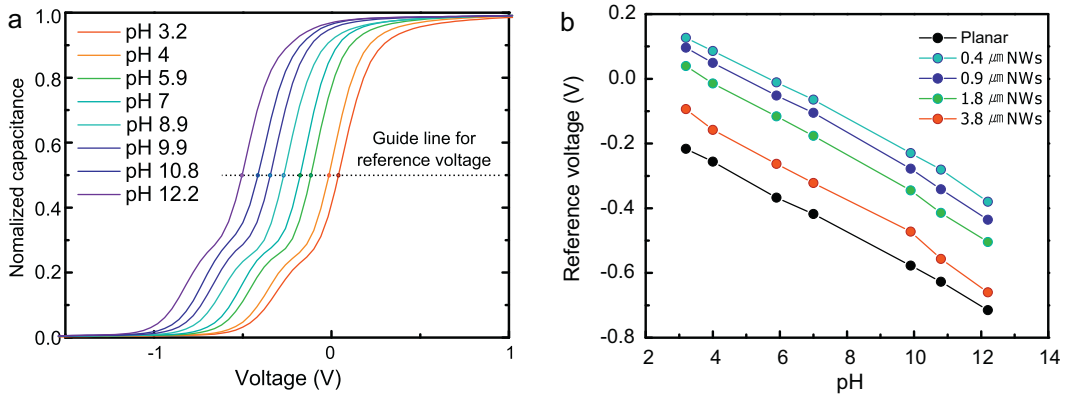

Fig. 6. (a) Normalized *C–V* curves measured from the EIS with 0.9 μm NWs. (b) Reference voltages of *C–V* curves for different pH buffer solutions with linear fitting lines.

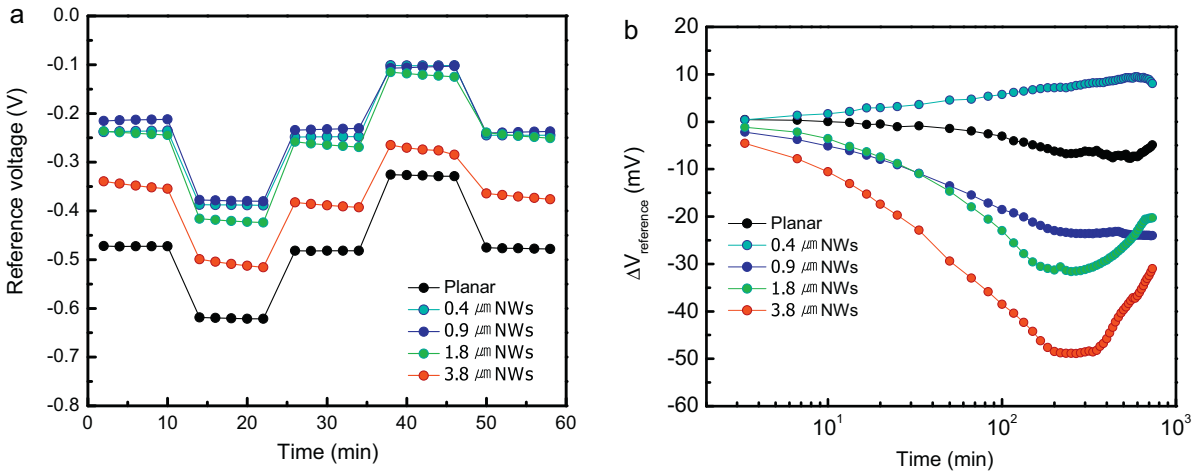

Fig. 7. (a) Hysteresis behavior for three pH buffer solutions. The sensors were subjected to the pH excursion of 7–10–7–4–7 for a period of 1 h. (b) Drift characteristics of the EIS sensors in a pH 7 buffer solution for 12 h.

is known to increase slowly and monotonically with time when sensors are submerged in electrolytes [29]. The hydration of the membrane (or gate) dielectric and the diffusion of ions in electrolyte to the dielectric are attributed to cause the drift effect [30]. In this work, the drift of the sensors was measured in a pH 7 buffer solution for 12 h at RT. In general, the drift property is compared by calculating the drift rate, $\Delta V_{reference}$/h. The drift rate in this work was, however, impossible to calculate and be compared to those of other references [10,11]. This is caused by a dynamic change instead of a monotonic increase or decrease in the drift curves with time as shown in Fig. 7b. The sensor with 0.4 μm NWs showed the most stable behavior in the drift with a positive shift while the other sensors including the planar type sensor presented a negative shift within 200 min. The drift of the sensors with 0.9 μm, 1.8 μm, 3.8 μm NWs shows turnarounds at about 200 min. In addition, the slopes of the drift curves before and after 200 min become larger for the sensors with longer NWs. Dynamic variation in the drift curves has been observed in some reports [11,27], however, the origins of the dynamic variation of the drift curves are not well-understood by the sensor community yet.

In conclusion, highly sensitive EIS sensors integrated with silicon NWs and Al_2O_3/SiO_2 stacked sensing membrane were demonstrated for the first time. The sensors exhibited higher capacitance as well as improved pH sensitivity compared to the planar type counterpart due to a noticeably increased surface area enabled by a high density of NWs. The observation of above-the-Nernstian-limit pH sensitivity was explained by the site-biding model. Slightly deteriorated hysteresis and drift properties of NW integrated EIS sensors were attributed to the increase in the number of trap sites in the larger surface areas of the NWs. The present work shows that integration of NWs into ISFETs can provide significantly higher sensing currents and improved signal-to-noise, which eventually allow for the fabrication of miniaturized high performance biochemical sensors.

Acknowledgment

This work is partially supported by NSF grant #0547679, a University of California CITRIS research grant and the Converging Research Center grant no. 2011K000694 funded by Korea Ministry of Education, Science and Technology.

References

[1] P. Bergveld, Development of an ion-sensitive solid-state device for neurophysiological measurements, IEEE Transactions on Biomedical Engineering BME–17 (1970) 70–71.
[2] A. Poghossian, et al., Possibilities and limitations of label-free detection of DNA hybridization with field-effect-based devices, Sensors and Actuators B: Chemical 111 (November) (2005) 470–480.
[3] W. Oelssner, et al., Encapsulation of ISFET sensor chips, Sensors and Actuators B: Chemical 105 (February) (2005) 104–117.
[4] M. Schöning, Playing around with field-effect sensors on the basis of EIS structures, LAPS and ISFETs, Sensors 5 (2005) 126–138.
[5] M. Schoning, et al., CIP (cleaning-in-place) suitable "non-glass" pH sensor based on a Ta_2O_5-gate EIS structure, Sensors and Actuators B: Chemical 111–112 (2005) 423–429.

[6] T.-M. Pan, K.-M. Liao, Comparison of structural and sensing characteristics of Pr_2O_3 and $PrTiO_3$ sensing membrane for pH-ISFET application, Sensors and Actuators B: Chemical 133 (2008) 97–104.
[7] L. Bousse, et al., Comparison of the hysteresis of Ta_2O_5 and Si_3N_4 pH-sensing insulators, Sensors and Actuators B: Chemical 17 (1994) 157–164.
[8] M.-H. Wu, et al., High dielectric constant PrY_xO_y sensing films electrolyte-insulator-semiconductor pH-sensor for the detection of urea, Analytica Chimica Acta 651 (2009) 36–41.
[9] W.J. Cho, H.J. Jang, High performance silicon-on-insulator based ion-sensitive field-effect transistor using high-k stacked oxide sensing membrane, Applied Physics Letters 99 (July) (2011).
[10] T.-M. Pan, K.-M. Liao, Structural properties and sensing characteristics of Y_2O_3 sensing membrane for pH-ISFET, Sensors and Actuators B: Chemical 127 (2007) 480–485.
[11] T.-M. Pan, et al., Structural properties and sensing performance of high-k Nd_2TiO_5 thin layer-based electrolyte-insulator-semiconductor for pH detection and urea biosensing, Biosensors and Bioelectronics 24 (2009) 2864–2870.
[12] M.-H. Wu, et al., Structural properties and sensing performance of high-k Sm_2O_3 membrane-based electrolyte-insulator-semiconductor for pH and urea detection, Sensors and Actuators B: Chemical 138 (2009) 221–227.
[13] T.-M. Pan, et al., Study of high-k Er_2O_3 thin layers as ISFET sensitive insulator surface for pH detection, Sensors and Actuators B: Chemical 138 (2009) 619–624.
[14] M.J. Schöning, et al., Novel electrochemical sensors with structured and porous semiconductor/insulator capacitors, Sensors and Actuators B: Chemical 65 (2000) 288–290.
[15] A. Simonis, et al., A long-term stable macroporous-type EIS structure for electrochemical sensor applications, Sensors and Actuators B: Chemical 91 (2003) 21–25.
[16] N. Zehfroosh, et al., High-sensitivity ion-selective field-effect transistors using nanoporous silicon, IEEE Electron Device Letters 31 (September) (2010) 1056–1058.
[17] M. Spijkman, Beyond the Nernst-limit with dual-gate ZnO ion-sensitive field-effect transistors, Applied Physics Letters 98 (2011) 043502.
[18] G. Jonghyun, et al., Beating the Nernst limit of 59 mV/pH with double-gated nano-scale field-effect transistors and its applications to ultra-sensitive DNA biosensors, in: 2010 IEEE International Electron Devices Meeting (IEDM), 2010, 8.7.1–8.7.4.
[19] J.C. Wang, et al., Reference electrode-insulator-nitride-oxide-semiconductor structure with Sm_2O_3 sensing membrane for pH-sensor application, Japanese Journal of Applied Physics 50 (April) (2011).
[20] K.Q. Peng, et al., Synthesis of large-area silicon nanowire arrays via self-assembling nanoelectrochemistry, Advanced Materials 14 (Aug 16 2002) 1164–1167.
[21] T. Qiu, P.K. Chu, Self-selective electroless plating: an approach for fabrication of functional 1D nanomaterials, Materials Science and Engineering: R: Reports 61 (2008) 59–77.
[22] C.S. Lai, et al., pH sensitivity improvement on 8 nm thick hafnium oxide by post deposition annealing, Electrochemical and Solid State Letters 9 (2006) G90–G92.
[23] L. Bousse, et al., Operation of chemically sensitive field-effect sensors as a function of the insulator-electrolyte interface, IEEE Transactions on Electron Devices 30 (1983) 1263–1270.
[24] M.J. Schöning, et al., Capacitive microsensors for biochemical sensing based on porous silicon technology, Sensors and Actuators B: Chemical 64 (2000) 59–64.
[25] T.M. Pan, K.M. Liao, Structural and sensing properties of high-k $PrTiO_3$ sensing membranes for pH-ISFET applications, IEEE Transactions on Biomedical Engineering 56 (February) (2009) 471–476.
[26] H.J. Jang, et al., Development of engineered sensing membranes for field-effect ion-sensitive devices based on stacked high-kappa dielectric layers, IEEE Electron Device Letters 32 (July) (2011) 973–975.
[27] H.J. Jang, W.J. Cho, High performance silicon-on-insulator based ion-sensitive field-effect transistor using high-k stacked oxide sensing membrane, Applied Physics Letters 99 (July) (2011).
[28] L. Bousse, et al., Hysteresis in Al_2O_3-gate ISFETs, Sensors and Actuators B: Chemical 2 (1990) 103–110.
[29] S. Jamasb, et al., A physical model for threshold voltage instability in Si_3N_4-gate H^+ sensitive FET's (pH ISFET's), IEEE Transactions on Electron Devices 45 (1998) 1239–1245.
[30] M.J. Schoning, et al., A highly long-term stable silicon-based pH sensor fabricated by pulsed laser deposition technique, Sensors and Actuators B: Chemical 35 (September) (Sep 1996) 228–233.

Biographies

Jin Yong Oh received the B.E. degree in chemical engineering from POSTECH in 2001 and the M.S. in materials science and engineering at GIST in 2005, Korea. He worked for Samsung Electronics semiconductor division in a flash memory development team for 5 years. Since 2009, he has been working toward the Ph.D degree in electrical engineering at University of California, Davis. His Ph.D study focuses on nanowire electronic devices including field effect transistors, and sensors. He authored/coauthored about 11 papers and holds 4 patents.

M. Saif Islam received the B.Sc. degree from Middle East Technical University (METU), Ankara, Turkey, in 1994, the M.Sc. degree from Bilkent University, Ankara, in 1996 (both in physics), and the M.S.E.E. and Ph.D. degrees in electrical engineering from the University of California, Los Angeles (UCLA), in 1999 and 2001. His research focuses on ultrafast nano-optoelectronic devices; synthesis, applications and device integration of semiconductor nanostructures for imaging, sensing, computing and energy conversion. He was at Hewlett–Packard Laboratories and Optical Network Research Laboratory, SDL Inc./JDS Uniphase Corporation. In 2004, he joined the University of California, Davis, where he is currently a Professor and Vice Chair. He has authored/coauthored more than 170 scientific papers, edited 15 books and conference proceeding, and holds 36 patents as an inventor/co-inventor. Dr. Islam is a member of the Optical Society of America, the Society of Photo-Optical Instrumentation Engineers, and the MRS. He received the National Science Foundation (NSF) Faculty Early Career Development Award in 2006, the UC Davis College of Engineering Outstanding Junior Faculty Award in 2006, the IEEE Professor of the Year Award (in 2005 and 2009), and the UC Davis Academic Senate Distinguished Teaching Award in 2010. He was the Chair/Co-Chair of 16 conferences and symposiums sponsored by MRS, IEEE, and SPIE.

Hyun-June Jang received the B.E. degree in electronic materials engineering from Kwangwoon University, Seoul, Korea, in 2011. His research interests are applications of the silicon-based biosensors, such as ISFET sensors. In the recent past, he published couple of papers about bio-sensors (EIS and ISFET) in several international journals. His current research is focusing on the realization of healthcare systems to monitor cell- or receptor binding-signal.

Won-Ju Cho received the B.S. degree from Kyungpook National University, Daegu, Korea, in 1989, and the M.S. and Ph.D degrees in electrical engineering from Keio University, Tokyo, Japan, in 1991 and 1994, respectively. In 1994, he joined HYNIX Semiconductor Inc., Cheongju-Si, Korea, where he was involved in the advanced process development of memory devices. From 1999 to 2000, he was with the AIST, Tsukuba, Japan, where he was involved in the development of ultra-low-loss power devices using silicon carbide. From 2000 to 2004, he joined ETRI, Daejon, Korea, where he is involved in research on nanoscale silicon devices. He was appointed as Professor of electronic material engineering at the Kwangwoon University, Seoul, Korea, in 2005. His current research interests include new electronic device materials, simulations, processing, and analysis of nanoscale semiconductor devices, biosensors. He has published more than 130 articles in international peer-reviewed scientific journals and more than 350 peer-reviewed conference proceedings.